JOURNAL OF CHEMICAL & ENGINEERING DATA

ARTICLE

pubs.acs.org/jced

Adsorption of Methylene Blue from Aqueous Solution with Activated Carbon/Cobalt Ferrite/Alginate Composite Beads: Kinetics, Isotherms, and Thermodynamics

Lunhong Ai,* Ming Li, and Long Li

Chemical Synthesis and Pollution Control Key Laboratory of Sichuan Province, College of Chemistry and Chemical Engineering, China West Normal University, Nanchong 637002, People's Republic of China

ABSTRACT: In this study, we have demonstrated a simple ionic polymerization route for the fabrication of a magnetically separable adsorbent, that is, activated carbon/cobalt ferrite/alginate composite beads, for effective dye removal from aqueous solution. Adsorption characteristics of the as-fabricated magnetic beads were assessed by using methylene blue (MB) as an adsorbate. The isotherms, kinetics, and thermodynamics of the adsorption of MB onto the magnetic beads have been studied at various experimental conditions (initial dye concentration, contact time, solution pH, and temperature). The kinetics of the adsorption process was found to follow the pseudosecond-order kinetics. The equilibrium data fitted well to both the Langmuir and the Freundlich models. Various thermodynamic parameters such as the standard Gibbs energy ($\Delta G°$), standard enthalpy ($\Delta H°$), and standard entropy ($\Delta S°$) changes were calculated. The prepared magnetic beads had a high magnetic sensitivity under an external magnetic field, which provides an easy and efficient way to separate the beads from aqueous solution.

1. INTRODUCTION

Dyestuff in wastewater from various industries, such as textiles, printing, pulp mills, leather, food, dyestuffs, and plastics, is stable and resistant to biodegradation because of its complex aromatic molecular structure.[1,2] Undoubtedly, the removal of dyestuff from waste effluents is of environmental importance. So far, various technologies including biological treatment,[3] coagulation/flocculation,[4] ozone treatment,[5] chemical oxidation,[6] membrane filtration,[7] ion exchange,[8] photocatalysis,[9] and adsorption[10] have been developed for the treatment of dye-containing effluents. Among them, adsorption is a reliable alternative due to its simplicity and high efficiency as well as the availability of a wide range of adsorbents (e.g., activated carbon, clay, biomass, polymer, zeolite, nanomaterials, etc.). In particular, activated carbon offers an attractive option for the efficient removal of various pollutants from waters because of its high surface area and porous structure.[11−14] Unfortunately, the utilization of activated carbon on a large scale is limited by process engineering difficulties, such as its dispersion problem and regeneration cost.

Supramolecular architectures of natural carbohydrates have recently received considerable attention as a suitable immobilization matrix in many fields, such as nanoengineering and biotechnology.[15,16] These biopolymers containing various functionalities, surface areas, and porosities are stable in most organic solvents, allowing them also to be suitable for environmental applications. Alginate, a natural polysaccharide extracted from brown seaweed, is a linear binary copolymer consisting of homopolymeric blocks of (1−4)-linked β-D-mannuronic acid (M) and α-L-guluronic acid (G) residues with a wide range of compositions and sequences (Figure 1a).[17,18] The most important feature of alginate lies on the selectively ionic interaction with multivalent ions to transform it into a hydrogel, forming the so-called "egg-box" structure.[19] Thereby, this cross-linked network endows it with significant advantages to use as an immobilization matrix for adsorbent (e.g., activated carbon) impregnation. In addition, the presence of negative carboxylate functions along polymer chains ensures its high affinity and binding capacity for cations. It can reasonably be utilized as a naturally available low cost adsorbent for water treatment.

More recently, many efforts have been devoted to the modified alginate-based adsorbent to introduce the as-combined components' functionality. For example, alginate/polyurethane composite foams with enhanced mechanical strength were capable of selectively adsorbing lead ions.[20] Chitosan−calcium alginate blended bioadsorbent was effective for the removal of various toxic organics (phenol,[21] *o*-chlorophenol,[21] 2,4-dichlorophenol,[22] and salicylic acid[22]) and heavy metals (Pb(II)[23] and Cu(II)[24]) from aqueous solutions. Besides these, as a suitable immobilization matrix, alginate can also entrap various compounds, such as activated carbon,[25] clay,[26] iron oxide,[27] and carbon nanotubes[28] to extend its functionality. A recent study by Rocher et al.[29,30] showed that the alginate beads containing commercially available activated carbon and magnetic iron oxide nanoparticles can be used as a low cost and biocompatible adsorbent, thus developing a clean and safe process for water pollution remediation. However, the fabrication route usually involved simply mixes activated carbon and iron oxide in a sodium alginate solution.

Previously, we have demonstrated the strong adsorbability and fast adsorption rate of the magnetically separable activated carbon/cobalt ferrite composite as a new adsorbent for water treatment.[31] Herein, we focus on the fabrication of magnetically separable activated carbon/cobalt ferrite/alginate composite beads as an efficient adsorbent for dye removal from aqueous solution. The objective of this study is to assess the removal efficiency of the selected dye model, methylene blue (MB), from aqueous solution onto the as-fabricated magnetic beads. Effects of various

Received: June 1, 2011
Accepted: June 29, 2011
Published: July 13, 2011

dx.doi.org/10.1021/je200536h | *J. Chem. Eng. Data* 2011, 56, 3475–3483

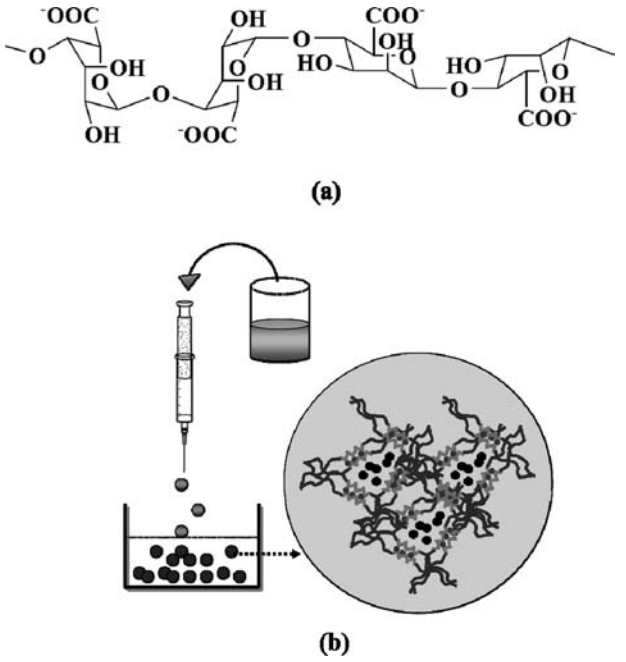

Figure 1. (a) Chemical structure of alginate and (b) schematic illustration for the fabrication of the magnetic beads.

parameters, namely, contact time, initial concentration, solution pH, and temperature, on the removal of MB were investigated in a batch mode. Kinetic, equilibrium, and thermodynamic studies have also been conducted.

2. EXPERIMENTAL SECTION

2.1. Chemicals. All of the reagents were of analytical grade with the mass fraction purity of 0.99 and used as received without further purification. $Co(NO_3)_2 \cdot 6H_2O$, $Fe(NO_3)_3 \cdot 9H_2O$, NaOH, $CaCl_2$, activated carbon (AC) powder, and methylene blue (MB) were purchased from Chengdu Kelong Chemical Reagent Co. (China). Sodium alginate, chemical grade with the mass fraction purity of 0.95, was obtained from Sinopharm Chemical Reagent Co., Ltd. (China). The activated carbon/cobalt ferrite ($CoFe_2O_4$) composite was obtained by a facile low-temperature refluxing route, according to our previous study.[31] The Brunauer−Emmett−Teller (BET) surface area and the total pore volume of the activated carbon/cobalt ferrite composite were determined to be 463 $m^2 \cdot g^{-1}$ and 0.18 $cm^3 \cdot g^{-1}$, respectively, by using a Micromeritics Gemini 2370 surface area analyzer at 77 K. The room temperature saturation magnetization was measured to be 7.6 $A \cdot m^2 \cdot kg^{-1}$ by using a Lakeshore 7404 vibrating sample magnetometer under the applied field of $\pm 1.2 \cdot 10^6$ $A \cdot m^{-1}$.

2.2. Preparation of the Activated Carbon/Cobalt Ferrite/Alginate Composite Beads. The activated carbon/cobalt ferrite/alginate composite beads were prepared by an ionic polymerization route. In a typical procedure, 1.5 g of sodium alginate powder was dissolved in 100 cm^3 deionized water at 353 K for $3.6 \cdot 10^3$ s, resulting in a transparent and viscous solution. A sample of 1.5 g of activated carbon/cobalt ferrite composite was then added to the above viscous solution and stirred for $1.8 \cdot 10^3$ s. The aqueous solution containing sodium alginate and activated carbon/cobalt ferrite composite was slowly added dropwise to 0.18 $mol \cdot kg^{-1}$ $CaCl_2$ solution using a syringe. The drops gelled into magnetic beads when they contacted the $CaCl_2$ solution. Finally, the resulting beads were washed several times with distilled water. A schematic illustration is shown in Figure 1b.

2.3. Adsorption Experiments. Batch adsorption experiments were carried out in a thermostatted shaker with a shaking speed of 15.7 $rad \cdot s^{-1}$ using 100 cm^3 Erlenmeyer flasks and conducted in duplicate. In general, 0.8 g of wet beads (corresponding dry weight of 0.07 g) were added into 25 cm^3 of MB solutions of desired initial concentrations [$(5.35 \cdot 10^{-5}$, $1.07 \cdot 10^{-4}$, $1.60 \cdot 10^{-4}$, $2.14 \cdot 10^{-4}$, and $2.67 \cdot 10^{-4}$) $mol \cdot kg^{-1}$] at natural pH in a flask and agitated in a temperature-controlled shaker at 298 K. At predetermined time intervals, the magnetic beads were removed from the solution by magnetic separation. The effect of pH on adsorption of MB onto the magnetic beads was studied over a pH range of (3.0 to 11) with a contact time of $7.2 \cdot 10^3$ s. The pH was adjusted by adding aqueous solutions of 0.1 $mol \cdot kg^{-1}$ HCl or 0.1 $mol \cdot kg^{-1}$ NaOH. The adsorption kinetics were determined by an analysis of the adsorption capacity from the aqueous solution at different time intervals. For adsorption isotherms, MB solution of different concentrations in the range of $(5.35 \cdot 10^{-5}$ to $2.67 \cdot 10^{-4})$ $mol \cdot kg^{-1}$ was incubated with magnetic beads under agitation until the equilibrium was achieved. The effect of temperature on the adsorption characteristics was investigated by determining the adsorption isotherms at (298, 308, 318, and 328) K. The concentration of dye was determined at 664 nm for MB using a UV−vis spectrophotometer (Shimadzu, UV-2550). The equilibrium adsorption capacity of MB onto the magnetic beads was calculated by the following equation:

$$q_e = \frac{(C_0 - C_e)V}{m} \quad (1)$$

where C_0 and C_e are the initial and equilibrium concentrations of MB, m is the mass of dry beads, and V is the volume of solution.

2.4. Characterization. The X-ray powder diffraction (XRPD) measurements were recorded on a Rigaku Dmax/Ultima IV diffractometer with monochromatized Cu Kα radiation (λ = 0.15418 nm). The morphology was observed with a JSM-6510 scanning electron microscope (SEM). A pHS-3C digital pH meter (Rex Instruments Factory, Shanghai, China) was employed for the pH measurements. The point of zero charge (pH_{PZC}) of the adsorbent was determined by the solid addition method. To a series of 100 cm^3 conical flasks, 45 cm^3 of 0.1 $mol \cdot kg^{-1}$ NaCl solution was transferred. The initial pH values (pH_i) of the solution were adjusted from (2.0 to 12) by adding either 0.1 $mol \cdot kg^{-1}$ HCl or 0.1 $mol \cdot kg^{-1}$ NaOH. The total volume of the solution in each flask was made exactly to 50 cm^3 by adding the NaCl solution. Then, 0.25 g of the dry magnetic beads was added to each flask, and the mixtures were agitated at 15.7 $rad \cdot s^{-1}$. After $1.73 \cdot 10^5$ s, the final pH values (pH_f) of the solutions were measured. The difference between the initial and final pH values ($\Delta pH = pH_i - pH_f$) was plotted against the pH_i. The point of intersection of the resulting curve with abscissa, at which $\Delta pH = 0$, gave the pH_{PZC}.

3. RESULTS AND DISCUSSION

3.1. Characterization of the Prepared Magnetic Beads. The crystalline structure of the magnetic composite beads was determined by X-ray powder diffraction (XRPD). Figure 2 shows the XRPD pattern of the magnetic beads. No peak observed for the calcium alginate and activated carbon indicates their amorphous nature. In contrast, the magnetic beads show the six characteristic

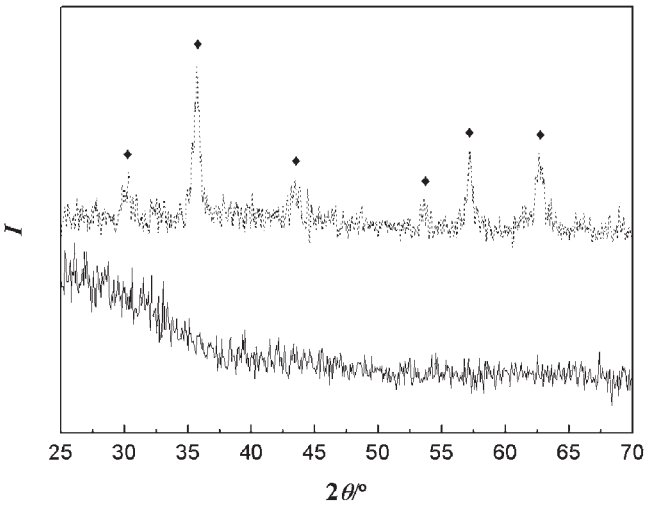

Figure 2. XRPD patterns (diffraction peak intensity I versus diffraction angle 2θ) of calcium alginate (solid line) and magnetic beads (dashed line). Diamond: $CoFe_2O_4$.

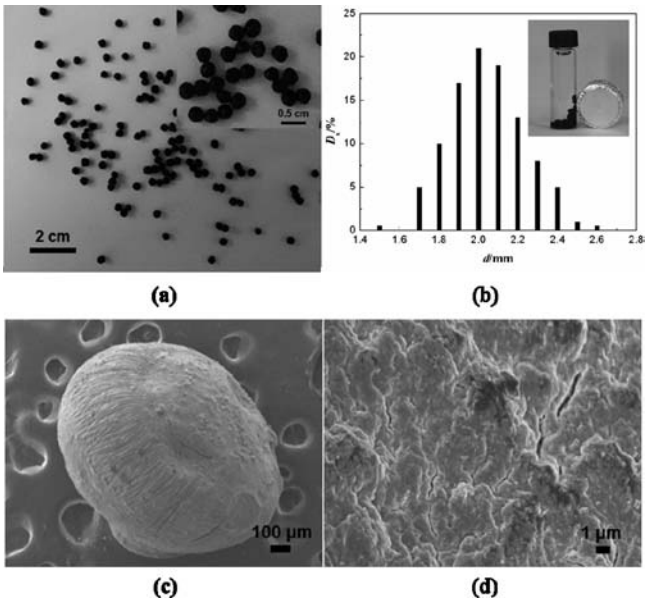

Figure 3. Digital photograph (a), size distribution D_s versus diameter d (b), and SEM image (c,d) of the magnetic beads. The inset in panel b shows the magnetic separation of the beads from solution under an external magnetic field.

peaks, which can be indexed to the cubic cobalt ferrite (JCPDS file no. 22-1086), suggesting that the cobalt ferrite in the magnetic beads is well-crystallized. Figure 3a shows a digital photograph of the wet magnetic beads, which display a quasi-spherical shape and dark brown color due to the presence of activated carbon/cobalt ferrite composite, indicating the well immobilization of activated carbon/cobalt ferrite composite in the matrix. The magnetic beads in the swollen state have average diameters of about 2 mm with a narrow distribution (Figure 3b). The surface morphology of the dry magnetic beads was observed by scanning electron microscopy (SEM). As shown in Figure 3c, the magnetic beads present an egg-like morphology. A magnified

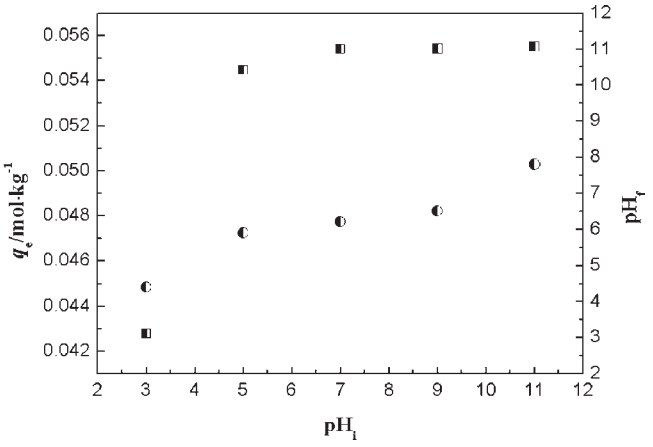

Figure 4. Equilibrium adsorption capacity q_e (half-filled square) and pH_f (half-filled circle) versus pH_i for the adsorption of MB onto the magnetic beads. pH_f: final pH values, pH_i: initial pH values.

SEM image (Figure 3d) further indicates the beads have a wrinkled and porous surface. This structural characteristic may be benefit for the uptake of toxic pollutants, such as organic dye in aqueous solution. Additionally, the beads possess a high magnetic response to an external magnetic field (inset in Figure 3b), which provides an easy and efficient way to separate the beads from aqueous solution.

3.2. Effect of pH. Solution pH is an important parameter in the adsorption process. In this study, the adsorption experiments have been conducted in the initial pH range of (3.0 to 11) with 25 cm^3 of $1.60 \cdot 10^{-4}$ $mol \cdot kg^{-1}$ initial concentration at 298 K for $7.2 \cdot 10^3$ s. Figure 4 shows the effect of the initial solution pH on the adsorption capacity of MB onto the magnetic beads. The adsorption capacity of MB experiences a rapid increase in the initial pH of (3.0 to 5.0), followed by a slow increase of at pH of (5.0 to 7.0) to an approximately constant at pH of (7.0 to 11). It is known that the solution pH can affect the surface charge of the adsorbent, the degree of ionization of the different pollutants, and the dissociation of functional groups on the active sites of the adsorbent as well as the structure of the dye molecule. For the magnetic beads, the point of zero charge (pH_{PZC}) determined by the solid addition method is about ca. 5.4 (Figure 5). Below this pH, the magnetic beads acquire a positive surface charge. The competitive effects of H^+ ions and the electrostatic repulsion between the cationic MB molecules and the positively charged active adsorption sites on the magnetic beads could lead to a decrease in the adsorption capacity of MB. It should be noted that leached Co and Fe from cobalt ferrite in the magnetic beads under acidic solution during the adsorption process possibly occurred.[32] In contrast, the surface of the magnetic beads acquires a negative charge at a pH higher than pH_{PZC}. The electrostatic attraction between the negatively charged surface of the magnetic beads and cationic MB molecule could result in an increase in the adsorption capacity of MB. Figure 4 also demonstrates that the solution pH values change during the adsorption process. At low initial pH ($pH_i \leq 5$), the final pH values (pH_f) are higher than pH_i values, which is due to an acid neutralization effect and proton adsorption of the surface of the magnetic beads.[33,34] The pH_f reaches (6.2 to 6.8) when the pH_i ranges from (7.0 to 11), indicating a buffering capacity caused by the adsorbent.[27,35,36]

3.3. Adsorption Kinetics. Figure 6 shows the effect of contact time on the adsorption capacity of MB onto the magnetic beads

at different initial concentrations at 298 K. It demonstrates that the adsorption capacity of MB increases rapidly at the initial adsorption stage and then continues to increase with contact time at a relatively slow rate. The adsorption process reaches equilibrium within $5.4 \cdot 10^3$ s, and no significant change is observed from ($5.4 \cdot 10^3$ to $1.08 \cdot 10^4$) s, suggesting that the adsorption rates are quite fast under all of the studied initial concentrations. The adsorption capacity of MB increases with increasing initial concentrations, since the initial concentrations provide an important driving force to overcome the mass transfer resistance of the dye molecules between the liquid phases and the solid phases.

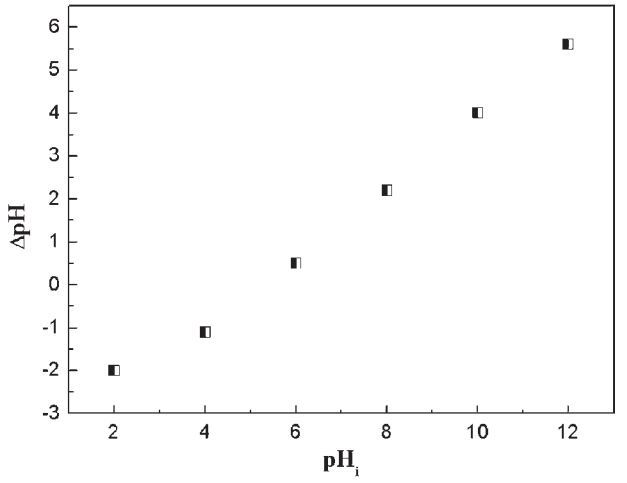

Figure 5. Plot of ΔpH versus pH_i for the determination of point of zero charge of the magnetic beads. ΔpH: the difference between the initial and final pH values, pH_i: initial pH values.

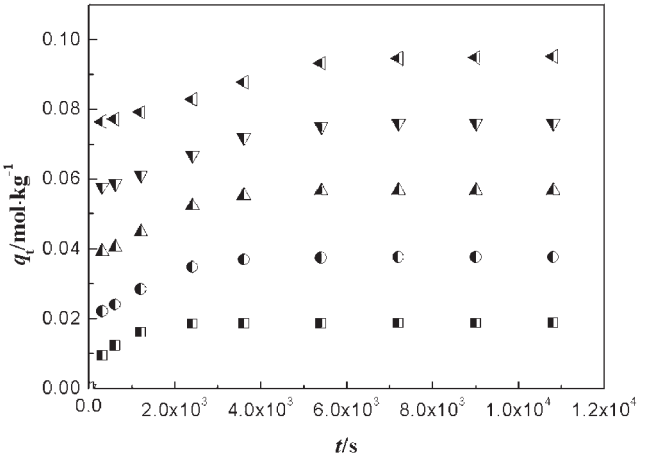

Figure 6. Adsorption capacity q_t versus time t for the adsorption of MB onto the magnetic beads at different initial concentrations (half-filled square, $5.35 \cdot 10^{-5}$ mol·kg^{-1}; half-filled circle, $1.07 \cdot 10^{-4}$ mol·kg^{-1}; half-filled up-triangle, $1.60 \cdot 10^{-4}$ mol·kg^{-1}; half-filled down-triangle, $2.14 \cdot 10^{-4}$ mol·kg^{-1}; half-filled left-triangle: $2.67 \cdot 10^{-4}$ mol·kg^{-1}).

To study the adsorption mechanism well, pseudofirst-order and pseudosecond-order equations were used to investigate the adsorption kinetics of MB onto the magnetic beads. In 1898, the first-order rate equation was represented by Lagergren for the adsorption of oxalic acid and malonic acid onto charcoal,[37] which assumes that the rate of change of solute uptake with time is directly proportional to difference in saturation concentration and the amount of solid uptake with time. The Lagergren pseudofirst-order kinetic model is expressed as:[37]

$$\log(q_e - q_t) = \log q_e - \frac{k_1 t}{2.303} \quad (2)$$

where k_1 is the pseudofirst-order rate constant and q_e and q_t are the adsorption capacity of MB onto the magnetic beads at equilibrium and at time t, respectively. The values of k_1 and q_e calculated from the slope and intercept of plots of $\log(q_e - q_t)$ versus t (not shown) are summarized in Table 1. The values of the correlation coefficients (R^2) for the pseudofirst-order model are relatively low, and the calculated q_e values ($q_{e,cal}$) are far from the experimental values ($q_{e,exp}$), indicating that the adsorption of MB onto the magnetic beads cannot be applied to a pseudofirst-order model, which is similar to the result reported for the adsorption of basic black dye onto calcium alginate beads.[38] In fact, in many cases the Lagergren pseudofirst-order equation could not fit well to the whole range of contact time and is generally applicable over the initial stage of the adsorption processes.[39,40]

In 1995, Ho proposed a law of the pseudosecond-order velocity that illustrates the velocity dependence on the capacity of adsorption in the solid phase but no dependence on the concentration of the adsorbed substance.[41] The pseudosecond-order kinetic model is presented as the following equation:[42]

$$\frac{t}{q_t} = \frac{1}{k_2 q_e^2} + \frac{t}{q_e} \quad (3)$$

where k_2 is the pseudosecond-order adsorption rate constant. The values of k_2 and q_e calculated from the slope and intercept of plots of t/q_t versus t (Figure 7) are given in Table 1. The correlation coefficients for the linear plots are very high ($R^2 > 0.99$), and the $q_{e,cal}$ values are in good agreement with $q_{e,exp}$ values, suggesting that the adsorption kinetics follows the

Table 1. Pseudofirst-Order and Pseudosecond-Order Model Parameters for the Adsorption of MB onto the Magnetic Beads

		pseudofirst-order			pseudosecond-order		
C_0	$q_{e,exp}$	k_1	$q_{e,cal}$		k_2	$q_{e,cal}$	
mol·kg^{-1}	mol·kg^{-1}	s^{-1}	mol·kg^{-1}	R^2	kg·mol^{-1}·s^{-1}	mol·kg^{-1}	R^2
$5.35 \cdot 10^{-5}$	0.019	$1.72 \cdot 10^{-4}$	0.008	0.910	0.223	0.019	0.999
$1.07 \cdot 10^{-4}$	0.037	$1.73 \cdot 10^{-4}$	0.023	0.984	0.087	0.039	1
$1.60 \cdot 10^{-4}$	0.057	$1.78 \cdot 10^{-4}$	0.032	0.979	0.074	0.058	1
$2.14 \cdot 10^{-4}$	0.076	$1.10 \cdot 10^{-4}$	0.027	0.949	0.052	0.078	0.999
$2.67 \cdot 10^{-4}$	0.095	$0.80 \cdot 10^{-4}$	0.026	0.952	0.043	0.097	0.999

pseudosecond-order model. Similar kinetics were observed in the adsorption of dye onto other magnetic calcium alginate-based adsorbents.[29,30,43] The $q_{e,cal}$ increases from (0.019 to 0.097) mol·kg^{-1} when the initial concentration of MB increases from (5.35·10^{-5} to 2.67·10^{-4}) mol·kg^{-1}, whereas the rate constants (k_2) values gradually decrease with the increase of initial concentrations due to strike hindrance of higher concentration of dye.[44]

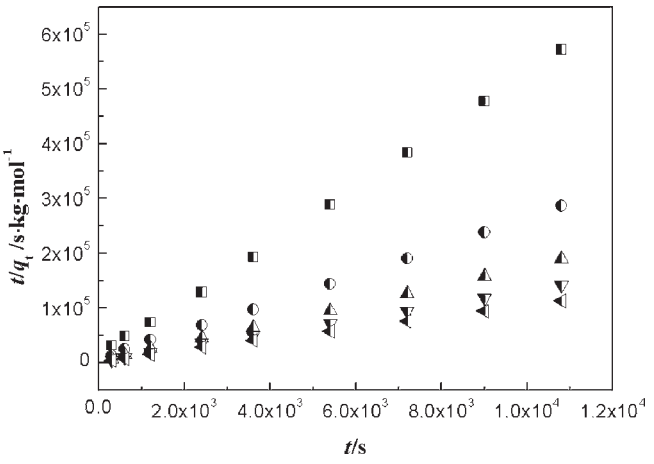

Figure 7. Pseudosecond-order plots of the ratio of time and adsorption capacity t/q_t versus time t for the adsorption of MB onto the magnetic beads (half-filled square, 5.35·10^{-5} mol·kg^{-1}; half-filled circle, 1.07·10^{-4} mol·kg^{-1}; half-filled up-triangle, 1.60·10^{-4} mol·kg^{-1}; half-filled down-triangle, 2.14·10^{-4} mol·kg^{-1}; half-filled left-triangle, 2.67·10^{-4} mol·kg^{-1}).

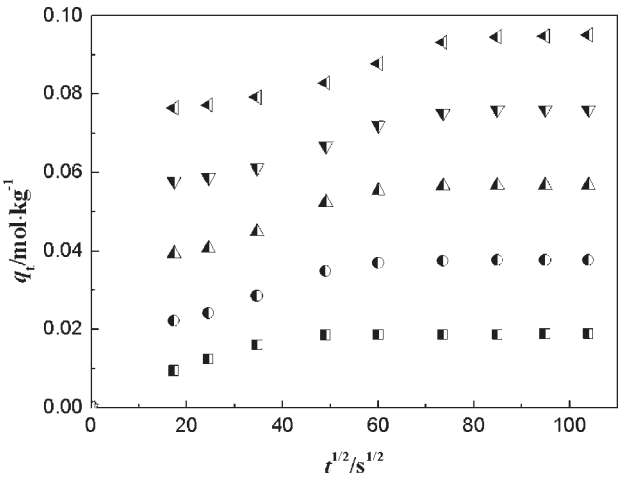

Figure 8. Intraparticle diffusion plots of adsorption capacity q_t versus the square root of time $t^{1/2}$ for the adsorption of MB onto the magnetic beads (half-filled square, 5.35·10^{-5} mol·kg^{-1}; half-filled circle, 1.07·10^{-4} mol·kg^{-1}; half-filled up-triangle, 1.60·10^{-4} mol·kg^{-1}; half-filled down-triangle, 2.14·10^{-4} mol·kg^{-1}; half-filled left-triangle, 2.67·10^{-4} mol·kg^{-1}).

From a mechanistic viewpoint, it is indispensable to identify the steps involved during adsorption process. In general, a solid−liquid adsorption process could be described by three steps: (i) transport of adsorbate from bulk solution through liquid film to the exterior surface of adsorbent (film diffusion); (ii) transport of adsorbate from the exterior surface to the pores of adsorbent (intraparticle diffusion); (iii) adsorption of adsorbate onto the active site in inner and outer surface of adsorbent. Commonly, the rate of adsorption is controlled by film diffusion or intraparticle diffusion or both. The intraparticle diffusion model can be used for identifying the steps involved during adsorption process, which is described as[45]

$$q_t = k_i t^{1/2} + C \quad (4)$$

where k_i is the intraparticle diffusion rate constant and C is a constant. It can be seen from eq 4 that, if intraparticle diffusion plays a significant role in controlling the kinetics of the adsorption process, the plots of q_t versus $t^{1/2}$ yield a straight line passing through the origin. As shown in Figure 8, three linear regions were clearly observed. The initial linear portion is a diffusion adsorption stage, resulting from the diffusion of dye through the solution to the external surface of adsorbent. The second linear portion is a gradual adsorption stage, corresponding to intraparticle diffusion of dye molecules through the pores of adsorbent. The third region is the final equilibrium stage where the intraparticle diffusion starts to slow down due to the extremely low adsorbate left in aqueous solution and the decrease of adsorption sites.[46] The observed multilinearity suggests that intraparticle diffusion is not the rate-limiting step. In addition, the slope of the linear portion implies the rate of the adsorption process. The diffusion rates (Table 2) decrease with the increase of the contact time under all of the studied initial dye concentrations. This is because the dye molecules diffuse into the inner structure of the adsorbent and the pores for diffusion become smaller. The free path of the molecules in the pore decreases, and the molecules may also be blocked. A similar phenomenon was observed in the adsorption of Reactive Black 5 onto activated carbons and basic dye onto pumpkin seed hull.[47,48]

The adsorption kinetic data were further analyzed by Boyd kinetic model to determine the actual rate-controlling step involved in the dye adsorption process. This model is expressed as[49]

$$F = 1 - \frac{6}{\pi^2}\exp(-B_t) \quad (5)$$

Table 2. Intraparticle Diffusion Model Parameters for the Adsorption of MB onto the Magnetic Beads

C_0	$k_{i,1}$	C_1		$k_{i,2}$	C_2		$k_{i,3}$	C_3	
mol·kg^{-1}	mol·kg^{-1}·s$^{-1/2}$	mol·kg^{-1}	R^2	mol·kg^{-1}·s$^{-1/2}$	mol·kg^{-1}	R^2	mol·kg^{-1}·s$^{-1/2}$	mol·kg^{-1}	R^2
5.35·10^{-5}	5.14·10^{-4}	1.26·10^{-4}	0.993	2.49·10^{-4}	0.007	0.911	4.36·10^{-6}	0.018	0.944
1.07·10^{-4}	1.04·10^{-3}	9.52·10^{-4}	0.907	2.30·10^{-4}	0.022	0.766	9.09·10^{-7}	0.038	0.951
1.60·10^{-4}	1.77·10^{-3}	1.96·10^{-3}	0.868	3.02·10^{-4}	0.034	0.842	4.92·10^{-6}	0.056	0.875
2.14·10^{-4}	2.57·10^{-3}	3.02·10^{-3}	0.852	3.66·10^{-4}	0.049	0.976	8.56·10^{-7}	0.076	0.957
2.67·10^{-4}	3.47·10^{-3}	4.04·10^{-3}	0.847	3.66·10^{-4}	0.066	0.976	2.72·10^{-5}	0.092	0.942

dx.doi.org/10.1021/je200536h |J. Chem. Eng. Data 2011, 56, 3475–3483

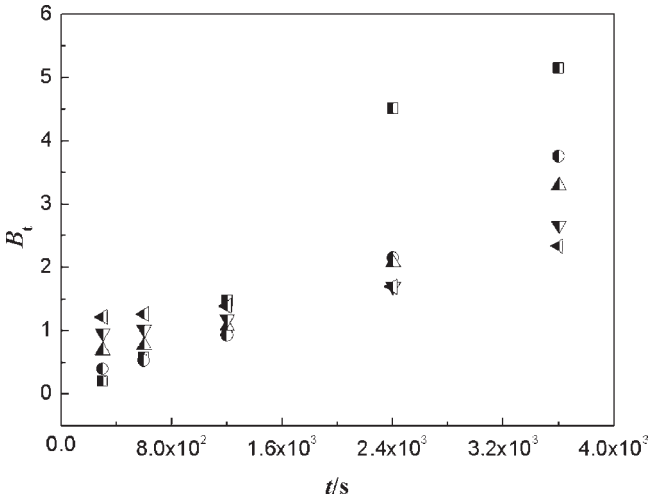

Figure 9. Plots of Boyd parameter B_t versus time t for the adsorption of MB onto the magnetic beads (half-filled square, $5.35 \cdot 10^{-5}$ mol·kg^{-1}; half-filled circle, $1.07 \cdot 10^{-4}$ mol·kg^{-1}; half-filled up-triangle, $1.60 \cdot 10^{-4}$ mol·kg^{-1}; half-filled down-triangle, $2.14 \cdot 10^{-4}$ mol·kg^{-1}; half-filled left-triangle, $2.67 \cdot 10^{-4}$ mol·kg^{-1}).

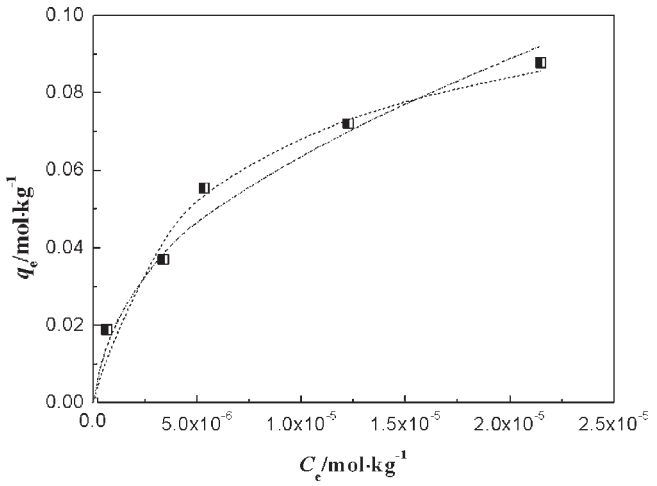

Figure 10. Equilibrium adsorption capacity q_e versus equilibrium concentrations C_e for the adsorption of MB onto the magnetic beads and predicted isotherm curves (half-filled square, experimental data; dashed line, Langmuir fitted curve; dash−dotted line, Freundlich fitted curve).

where F is the fraction of solute adsorbed at different time t and parameter B_t is a mathematical function of F and is given by

$$F = \frac{q_t}{q_e} \tag{6}$$

In the substitution of eq 6 in eq 5, the kinetic expression can be represented as

$$B_t = -0.4977 - \ln(1 - F) \tag{7}$$

The linearity of these plots is employed to distinguish between external transport (film diffusion) and intraparticle transport controlled rates of adsorption. A straight line passing through the origin proves that adsorption processes are governed by intraparticle diffusion mechanism; otherwise they are governed by film diffusion or external mass transport.[50] As shown in Figure 9, the plots are linear but do not pass through the origin, and the R^2 of linear fitting at different initial dye concentration is in the range of (0.935 to 0.976), indicating that external mass transport mainly governs the rate-limiting process of adsorption of MB onto the magnetic beads.

Table 3. Isotherm Parameters for the Adsorption of MB onto the Magnetic Beads

Langmuir			Freundlich		
b	q_m		K_f		
kg·mol^{-1}	mol·kg^{-1}	R^2	mol·kg^{-1}	n	R^2
$2.116 \cdot 10^5$	0.105	0.973	0.036	2.19	0.979

3.4. Adsorption Isotherms. The isotherm study can describe how an adsorbate interacts with the adsorbent. The isotherm provides a relationship between the concentration of dye in solution and the amount of dye adsorbed on the solid phase when both phases are in equilibrium. Figure 10 shows the equilibrium isotherms for the adsorption of MB onto the magnetic beads, and the equilibrium adsorption data are analyzed by using the Langmuir and Freundlich isotherm models.[51,52] The Langmuir isotherm theory assumes monolayer coverage of adsorbate over a homogeneous adsorbent surface. A basic assumption is that adsorption takes place at specific homogeneous sites within the adsorbent. Once a dye molecule occupies a site, no further adsorption can take place at that site. The Langmuir isotherm is

$$\frac{C_e}{q_e} = \frac{1}{bq_m} + \frac{C_e}{q_m} \tag{8}$$

where b is the Langmuir constant related to the energy of adsorption, and q_m is the Langmuir monolayer adsorption capacity. The values of q_m and b are calculated from the slope and intercept of the linear plot of C_e/q_e against C_e, and the parameters are shown in Table 3. The correlation coefficient of the isotherm is relatively high ($R^2 = 0.973$), which indicates that the Langmuir model is suitable for describing the adsorption equilibrium of MB by the magnetic beads. The monolayer adsorption capacity determined from the Langmuir isotherm is 0.105 mol·kg^{-1}.

The essential characteristics of the Langmuir isotherm can be expressed in terms of a dimensionless constant separation factor R_L that is given by[53]

$$R_L = \frac{1}{1 + bC_0} \tag{9}$$

The value of R_L indicates the shape of the isotherm to be either unfavorable ($R_L > 1$), linear ($R_L = 1$), favorable ($0 < R_L < 1$), or irreversible ($R_L = 0$).[54] The calculated R_L values at different initial concentrations of MB are presented in Figure 11. The values of R_L lie between 0 and 1, thereby confirming that the adsorption is a favorable process. In addition, the low R_L values reveal that the interaction between dye molecules and the magnetic beads might be relatively strong.[55]

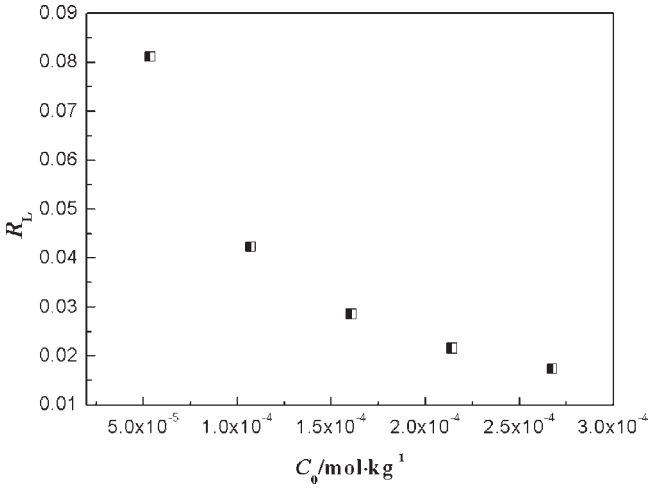

Figure 11. Separation factor R_L versus initial concentrations C_0 for the adsorption of MB onto the magnetic beads.

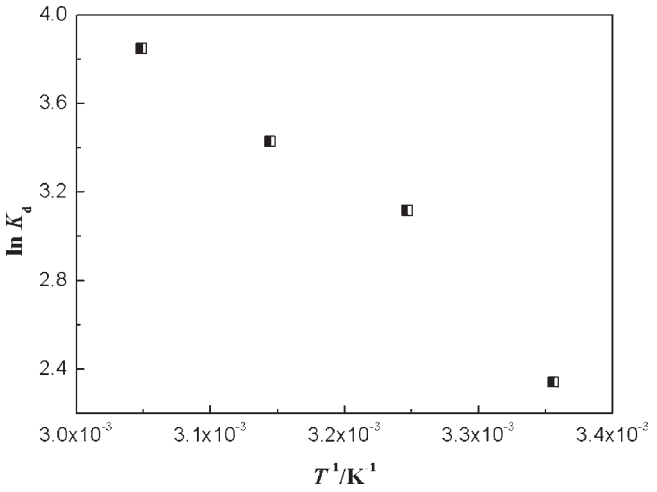

Figure 12. van't Hoff plot of the natural logarithm of the distribution coefficient ln K_d versus the reciprocal of temperature T^{-1} for the adsorption of MB onto the magnetic beads.

The Freundlich isotherm is an empirical equation assuming that the adsorption process takes place on heterogeneous surfaces and adsorption capacity is related to the concentration of dye at equilibrium. It can be described as:

$$\log q_e = \log K_f + \frac{1}{n}\log C_e \quad (10)$$

where K_f is roughly an indicator of the adsorption capacity and $1/n$ is the adsorption intensity. Freundlich constants K_f and n can be obtained from the intercept and the slope of the linear plot of log q_e versus log C_e (Table 3). The correlation coefficient (R^2 = 0.979) reflects that the experimental data agree with the Freundlich mode. Meanwhile, the value of n for Freundlich model is greater than 1, indicating that the adsorption of MB also exhibits a favorable shape.

3.5. Adsorption Thermodynamics. The thermodynamic parameters provide in-depth information on inherent energetic changes that are associated with adsorption. The thermodynamic parameters, such as standard Gibbs energy change ($\Delta G°$), enthalpy change ($\Delta H°$), and entropy change ($\Delta S°$), were determined by using the following equations:[56]

Table 4. Thermodynamic Parameters for the Adsorption of MB onto the Magnetic Beads

T	$\Delta G°$	$\Delta H°$	$\Delta S°$
K	kJ·mol^{-1}	kJ·mol^{-1}	J·mol^{-1}·K^{-1}
298	−5.80	39.4	152
308	−7.98		
318	−9.06		
328	−10.5		

$$K_d = \frac{q_e}{C_e} \quad (11)$$

$$\Delta G^o = -RT \ln K_d \quad (12)$$

$$\ln K_d = \frac{\Delta S^o}{R} - \frac{\Delta H^o}{RT} \quad (13)$$

where K_d is the distribution coefficient, T is the temperature, and R is the gas constant (8.3145 J·mol^{-1}·K^{-1}), respectively. $\Delta S°$ and $\Delta H°$ are calculated from the slope and intercept of van't Hoff plots of ln K_d versus T^{-1} (Figure 12). The calculated values of thermodynamic parameters are given in Table 4. The negative $\Delta G°$ values at different temperatures indicate the spontaneous nature of the adsorption of MB onto the magnetic beads. The more negative value with the increase of temperature shows that the amount adsorbed at equilibrium must increase with increasing temperature. The value of $\Delta H°$ is found to be positive in the temperature range of (298 to 328) K. Adsorption in liquid phase is a complex phenomenon in which solute and solvent compete for the solid surface. Adsorption and desorption of solute and solvent molecules take place simultaneously, and the energetic changes involved could result in a positive $\Delta H°$. In addition, the positive value of $\Delta S°$ reflects the good affinity of MB toward the magnetic beads and the increased randomness at the solid−solution interface during the adsorption process.

4. CONCLUSION

In conclusion, a novel magnetically separable adsorbent, namely, activated carbon/cobalt ferrite/alginate composite beads, has been prepared by a simple ionic polymerization route. Adsorption characteristics of the as-fabricated magnetic beads were assessed by using methylene blue (MB) as an adsorbate. The pH effect, kinetics, isotherms, and thermodynamics are determined by batch experiments. The kinetic studies reveal that the adsorption process follows the pseudosecond-order kinetic model. The equilibrium data have been well-described by the Langmuir and Freundlich models. The $\Delta H°$ value is positive in the temperature range of (298 to 328) K. The $\Delta G°$ values are negative at different temperatures indicating the spontaneous nature of the adsorption of MB onto the magnetic beads. The $\Delta S°$ value is positive suggesting the good affinity of MB toward the magnetic beads and the increased randomness at the solid−solution interface during the adsorption process. In addition, the prepared magnetic beads have high magnetic sensitivity under an external magnetic field, which provides an easy and efficient way to separate the beads from aqueous solution.

AUTHOR INFORMATION

Corresponding Author

*E-mail: ah_aihong@163.com. Tel.: 86-817-2568081. Fax: 86-817-2224217.

Funding Sources

This work was supported by Program for Scientific and Technological Innovative Team in Sichuan Provincial Universities (2010008), Open Project of Chemical Synthesis and Pollution Control Key Laboratory of Sichuan Province (11CSPC-(1-7)), and Program for Scientific Research Innovation Team of China West Normal University.

REFERENCES

(1) El Qada, E. N.; Allen, S. J.; Walker, G. M. Adsorption of basic dyes from aqueous solution onto activated carbons. *Chem. Eng. J.* **2008**, *135*, 174–184.

(2) Han, R.; Ding, D.; Xu, Y.; Zou, W.; Wang, Y.; Li, Y.; Zou, L. Use of rice husk for adsorption of congo red from aqueous solution in column made. *Bioresour. Technol.* **2008**, *99*, 2938–2946.

(3) Kornaros, M.; Lyberatos, G. Biological treatment of wastewaters from a dye manufacturing company using a trickling filter. *J. Hazard. Mater.* **2006**, *136*, 95–102.

(4) Lee, J. W.; Choi, S. P.; Thiruvenkatachari, R.; Shim, W. G.; Moon, H. Submerged microfiltration membrane coupled with alum coagulation/powder activated carbon adsorption for complete decolorization of reaction dye. *Water Res.* **2006**, *40*, 435–444.

(5) Selcuk, H. Decolorization, detoxification of textile wastewater by ozonation and coagulation processes. *Dyes Pigm.* **2005**, *64*, 217–222.

(6) Dutta, K.; Mukhopadhyaya, S.; Bhattacharjee, S.; Chaudhuri, B. Chemical oxidation of methylene blue using a Fenton-like reaction. *J. Hazard. Mater.* **2001**, *84*, 57–71.

(7) Buonomenna, M. G.; Gordano, A.; Golemme, G.; Drioli, E. Preparation, characterization and use of PEEKWC nanofiltration membranes for removal of Azur B dye from aqueous media. *React. Funct. Polym.* **2009**, *69*, 259–263.

(8) Liu, C. H.; Wu, J. S.; Chiu, H. C.; Suen, S. Y.; Chu, K. H. Removal of anionic reactive dyes from water using anion exchange membranes as adsorbers. *Water Res.* **2007**, *41*, 1491–1500.

(9) Muruganandham, M.; Swaminathan, M. TiO_2-UV photocatalytic oxidation of Reactive Yellow 14: Effect of operational parameters. *J. Hazard. Mater.* **2006**, *135*, 78–86.

(10) Arami, M.; Yousefi-Limaee, N.; Mahmoodi, N. M.; Salman-Tabrizi, N. Equilibrium and kinetics studies for the adsorption of direct and acid dyes from aqueous solution by soy meal hull. *J. Hazard. Mater.* **2006**, *B135*, 171–179.

(11) Martyn-Gullon, I.; Font, R. Dynamic pesticide removal with activated carbon fibers. *Water Res.* **2001**, *35*, 516–520.

(12) Pendleton, P.; Wu, S. H. Kinetics of dodecanoic acid adsorption from caustic solution by activated carbon. *J. Colloid Interface Sci.* **2003**, *226*, 245–250.

(13) Garner, I. A.; Watson-Craik, I. A.; Kirkwood, R. Dual solute adsorption of 2,4,6-trichlorophenol and *N*-[2-(2,4,6-trichlorophenoxy)propyl]amine onto activated carbon. *J. Chem. Technol. Biotechnol.* **2001**, *76*, 932–940.

(14) Pelekani, C.; Snoeyink, V. L. A kinetic and equilibrium study of competitive adsorption between atrazine and congo red dye on activated carbon: The importance of pore size distribution. *Carbon* **2001**, *39*, 25–37.

(15) Bandyopadhyaya, R.; Nativ-Roth, E.; Regev, O.; Yerushalmi-Rozen, R. Stabilization of individual carbon nanotubes in aqueous solutions. *Nano Lett.* **2002**, *2*, 25–28.

(16) Finotelli, P. V.; Morales, M. A.; Rocha-Leão, M. H.; Baggio-Saitovitch, E. M.; Rossi, A. M. Magnetic studies of iron(III) nanoparticles in alginate polymer for drug delivery applications. *Mater. Sci. Eng., C* **2004**, *24*, 625–629.

(17) Draget, K. I.; Taylor, C. Chemical, physical and biological properties of alginates and their biomedical implications. *Food Hydrocolloids* **2011**, *25*, 251–256.

(18) Fuks, L.; Filipiuk, D.; Majdan, M. Transition metal complexes with alginate biosorbent. *J. Mol. Struct.* **2006**, *792−793*, 104–109.

(19) Grant, G. T.; Morris, E. R.; Rees, D. A.; Smith, P. J. C.; Thom, D. Biological interactions between polysaccharides and divalent cations: The egg-box model. *FEBS Lett.* **1973**, *32*, 195–198.

(20) Sone, H.; Fugetsu, B.; Tanaka, S. Selective elimination of lead(II) ions by alginate/polyurethane composite foams. *J. Hazard. Mater.* **2009**, *162*, 423–429.

(21) Nadavala, S. K.; Swayampakula, K.; Boddu, V. M.; Abburi, K. Biosorption of phenol and o-chlorophenol from aqueous solutions onto chitosan-calcium alginate blended beads. *J. Hazard. Mater.* **2009**, *162*, 482–489.

(22) Ding, Y.; Zhao, Y.; Tao, X.; Zheng, Y.-Z.; Chen, J.-F. Assembled alginate/chitosan micro-shells for removal of organic pollutants. *Polymer* **2009**, *50*, 2841–2846.

(23) Ngah, W. S. W.; Fatinathan, S. Pb(II) biosorption using chitosan and chitosan derivatives beads: Equilibrium, ion exchange and mechanism studies. *J. Environ. Sci.* **2010**, *22*, 338–346.

(24) Ngah, W. S. W.; Fatinathan, S. Adsorption of Cu(II) ions in aqueous solution using chitosan beads, chitosan-GLA beads and chitosan-alginate beads. *Chem. Eng. J.* **2008**, *143*, 62–72.

(25) Park, H. G.; Kim, T. W.; Chae, M. Y.; Yoo, I.-K. Activated carbon-containing alginate adsorbent for the simultaneous removal of heavy metals and toxic organics. *Process Biochem.* **2007**, *42*, 1371–1377.

(26) Lezehari, M.; Basly, J.-P.; Baudu, M.; Bouras, O. Alginate encapsulated pillared clays: Removal of a neutral/anionic biocide (pentachlorophenol) and a cationic dye (safranine) from aqueous solutions. *Colloids Surf., A* **2010**, *366*, 88–94.

(27) Wu, D.; Zhao, J.; Zhang, L.; Wu, Q.; Yang, Y. Lanthanum adsorption using iron oxide loaded calcium alginate beads. *Hydrometallurgy* **2010**, *101*, 76–83.

(28) Li, Y.; Liu, F.; Xia, B.; Du, Q.; Zhang, P.; Wang, D.; Wang, Z.; Xia, Y. Removal of copper from aqueous solution by carbon nanotube/calcium alginate composites. *J. Hazard. Mater.* **2010**, *177*, 876–880.

(29) Rocher, V.; Siaugue, J.-M.; Cabuil, V.; Bee, A. Removal of organic dyes by magnetic alginate beads. *Water Res.* **2008**, *42*, 1290–1298.

(30) Rocher, V.; Bee, A.; Siaugue, J.-M.; Cabuil, V. Dye removal from aqueous solution by magnetic alginate beads crosslinked with epichlorohydrin. *J. Hazard. Mater.* **2010**, *178*, 434–439.

(31) Ai, L.; Huang, H.; Chen, Z.; Wei, X.; Jiang, J. Activated carbon/$CoFe_2O_4$ composites: Facile synthesis, magnetic performance and their potential application for the removal of malachite green from water. *Chem. Eng. J.* **2010**, *156*, 243–249.

(32) Zhang, S.; Niu, H.; Cai, Y.; Zhao, X.; Shi, Y. Arsenite and arsenate adsorption on coprecipitated bimetal oxide magnetic nanomaterials: $MnFe_2O_4$ and $CoFe_2O_4$. *Chem. Eng. J.* **2010**, *158*, 599–607.

(33) Sathishkumar, M.; Binupriya, A. R.; Kavitha, D.; Selvakumar, R.; Jayabalan, R.; Choi, J. G.; Yun, S. E. Adsorption potential of maize cob carbon for 2,4-dichlorophenol removal from aqueous solutions: Equilibrium, kinetics and thermodynamics modeling. *Chem. Eng. J.* **2009**, *147*, 265–271.

(34) Mane, V. S.; Babu, P. V. V. Studies on the adsorption of brilliant green dye from aqueous solution onto low-cost NaOH treated saw dust. *Desalination* **2011**, *273*, 321–329.

(35) Lim, S. F.; Zheng, Y. M.; Zou, S. W. Characterization of copper adsorption onto an alginate encapsulated magnetic sorbent by a combined FT-IR, XPS, and mathematical modeling study. *Environ. Sci. Technol.* **2008**, *42*, 2551–2556.

(36) Chen, J. P.; Wang, L. Characterization of a Ca-alginate based ion-exchange resin and its applications in lead, copper, and zinc removal. *Sep. Sci. Technol.* **2001**, *36*, 3617–3637.

(37) Lagergren, S. About the theory of so-called adsorption of soluble substances. *K. Sven. Vetenskapsakad. Handl.* **1898**, *24*, 1–39.

(38) Aravindhan, R.; Fathima, N. N.; Rao, J. R.; Nair, B. U. Equilibrium and thermodynamic studies on the removal of basic black dye using calcium alginate beads. *J. Hazard. Mater.* **2007**, *299*, 232–238.
(39) McKay, G.; Ho, Y. S. The sorption of lead (II) on peat. *Water Res.* **1999**, *33*, 578–584.
(40) Bulut, E.; Ozacar, M.; Sengil, I. A. Adsorption of malachite green onto bentonite: Equilibrium and kinetic studies and process design. *Microporous Mesoporous Mater.* **2008**, *115*, 234–246.
(41) Ho, Y. S. Adsorption of heavy metals from waste streams by peat. Ph.D. Thesis, University of Birmingham, Birmingham, U.K., 1995.
(42) Ho, Y. S.; McKay, G. Sorption of dye from aqueous solution by peat. *Chem. Eng. J.* **1998**, *70*, 115–124.
(43) Ngomsik, A.-F.; Bee, A.; Siaugue, J.-M.; Talbot, D.; Cabuil, V.; Cote, G. Co(II) removal by magnetic alginate beads containing Cyanex 272. *J. Hazard. Mater.* **2009**, *166*, 1043–1049.
(44) Gad, H. M. H.; El-Sayed, A. A. Activated carbon from agricultural by-products for the removal of Rhodamine-B from aqueous solution. *J. Hazard. Mater.* **2009**, *168*, 1070–1081.
(45) Weber, W. J., Jr.; Morris, J. C. Kinetics of adsorption on carbon from solution. *J. Sanit. Eng. Div. Am. Soc., Civ. Eng.* **1963**, *89*, 31–60.
(46) Wang, X.; Pan, J.; Guan, W.; Dai, J.; Zou, X.; Yan, Y.; Li, C.; Hu, W. Selective removal of 3-chlorophenol from aqueous solution using surface molecularly imprinted microspheres. *J. Chem. Eng. Data* **2011**, *56*, 2793–2801.
(47) Ip, A. W. M.; Barford, J. P.; McKay, G. A comparative study on the kinetics and mechanisms of removal of Reactive Black 5 by adsorption onto activated carbons and bone char. *Chem. Eng. J.* **2010**, *157*, 434–442.
(48) Hameeda, B. H.; El-Khaiary, M. I. Removal of basic dye from aqueous medium using a novel agricultural waste material: Pumpkin seed hull. *J. Hazard. Mater.* **2008**, *155*, 601–609.
(49) Boyd, G. E.; Adamson, A. W.; Meyers, L. S. The exchange adsorption of ions from aqueous solutions by organic zeolites: II kinetics. *J. Am. Chem. Soc.* **1947**, *69*, 2836–2848.
(50) El-Kamash, A. M.; Zaki, A. A.; Abed-El-Geleel, M. Modeling batch kinetics and thermodynamics of zinc and cadmium removal from waste solutions using synthetic zeolite. *J. Hazard. Mater.* **2005**, *127*, 211–220.
(51) Langmuir, I. The constitution and fundamental properties of solids and liquids. *J. Am. Chem. Soc.* **1916**, *38*, 2221–2295.
(52) Freundlich, H. M. F. Over the adsorption in solution. *Z. Phys. Chem.* **1906**, *57*, 385–471.
(53) Weber, T. W.; Chakravorti, R. K. Pore and solid diffusion models for fixed-bed adsorbers. *AIChE J.* **1974**, *20*, 228–238.
(54) McKay, G. Adsorption of dyestuffs from aqueous solution with activated carbon. I. equilibrium and batch contact time studies. *J. Chem. Technol. Biotechnol.* **1982**, *32*, 759–772.
(55) Xiong, L.; Yang, Y.; Mai, J.; Sun, W.; Zhang, C.; Wei, D.; Chen, Q.; Ni, J. Adsorption behavior of methylene blue onto titanate nanotubes. *Chem. Eng. J.* **2010**, *156*, 313–320.
(56) Hameed, B. H.; Ahmad, A. A. Batch adsorption of methylene blue from aqueous solution by garlic peel, an agricultural waste biomass. *J. Hazard. Mater.* **2009**, *164*, 870–87.